Electrostatic Potential Compact Model for Symmetric and Asymmetric Lightly Doped DG-MOSFET Devices

H. Abebe*, E. Cumberbatch**, S. Uno*** and V. Tyree*

*USC Viterbi School of Engineering, Information Sciences Institute, MOSIS service,
Marina del Rey, CA 90292, USA. Tel: (310) 448-8740, Fax: (310) 823-5624,
e-mail: abebeh@mosis.com and tyree@mosis.com
**Claremont Graduate University, School of Mathematical Sciences,
710 N College Ave, Claremont, CA 91711, USA. Tel: (909) 607-3369,
Fax: (909) 621-8390, e-mail: ellis.cumberbatch@cgu.edu
***Nagoya University, Department of Electrical and Computer Engineering, Japan
Tel: +81-52-789-2794, Fax: +81-52-789-3139, e-mail: uno@nuee.nagoya-u.ac.jp

ABSTRACT

This work is a continuation of [1, 2]. The analytical *symmetric* and *asymmetric* lightly doped DG-MOSFET device electrostatic potential compact model presented here improves the compact model accuracy without any *iteration*. The model is developed using the *Lambert Function* and a 2-dimensional (2-D) parabolic electrostatic potential approximation across the device is assumed. Our compact models are compared with the 2-D numerical data from *Sentaurus* [3] and give excellent results

Keywords: circuit simulation, compact device modeling, MOSFET, SPICE

1 INTRODUCTION

DG-MOSFET device architecture is promising to overcome the short channel effects for CMOS scaling into the sub-30 nm regime. Although there are some publications on compact modeling of the DG-MOSFET, most of the work is focusing on symmetric and undoped DG-MOSFET devices such as [6] and [7]. Some asymmetric DG-MOSFET compact models in the literature such as [8-10] usually consider the asymmetry arises only from different flatband voltages and oxide thicknesses at the two gates. In [2] we tried to address asymmetry due to different oxide thicknesses, flatband voltages and applied gate voltages at the two input gate terminals altogether. But our simulation of the asymmetric devices at different back and front gate biases indicates that the model accuracy deteriorates rapidly out of the linear region as saturation takes over. In this paper we improved the electrostatic potential compact model accuracy of [2] in the saturation region.

2 COMPACT DG-MOSFET MODELS

The Poisson equation for the electrostatic potential $\psi(X,Y)$ in uniformly doped silicon is

$$\frac{d^2\psi}{dX^2} + \frac{d^2\psi}{dY^2} = \frac{q}{\varepsilon_s}\left(n_i e^{q(\psi - V)/kT} + N_a\right) \tag{1}$$

where q represents electron charge, ε_s semiconductor permittivity, V quasi-Fermi potential: $V=0$ at the source and $V=V_{ds}$ at the drain, N_a silicon doping, k Boltzmann constant, T temperature, X direction perpendicular to the channel at the mid-section, Y direction along the channel from the source end, n_i intrinsic density and the electron density is $n = n_i e^{(\psi - V)/V_{th}}$.

The continuity of the electric displacement at the silicon/silicon-oxide interfaces gives the boundary conditions as

$$\varepsilon_s \left.\frac{\partial\psi}{\partial X}\right|_{X=\frac{T_s}{2}} = \varepsilon_{ox}\left(\frac{V_{gf} - \psi_{sf} - \Delta\phi_f}{T_{oxf}}\right),$$

$$\varepsilon_s \left.\frac{\partial\psi}{\partial X}\right|_{X=\frac{-T_s}{2}} = -\varepsilon_{ox}\left(\frac{V_{gb} - \psi_{sb} - \Delta\phi_b}{T_{oxb}}\right) \tag{2}$$

where V_{gf}, V_{gb} are front and back gate voltages; ψ_{sf}, ψ_{sb} surface potentials; T_{oxf}, T_{oxb} oxide thicknesses; $\Delta\phi_f$, $\Delta\phi_b$ work function differences or flat band voltages, and ε_{ox} oxide permittivity.

Using the scaled variables below, the Poisson equation (1) is rewritten as

$$\frac{\partial^2 w}{\partial x^2}+\varepsilon^2\frac{\partial^2 w}{\partial y^2}=\frac{1}{\lambda}e^{(w-v)\ln\lambda}+1 \tag{3}$$

where $\varepsilon=\frac{L_d}{L}\sqrt{\ln\lambda/\lambda}$, $L_d=\sqrt{\frac{V_{th}\varepsilon_s}{n_i q}}$ is the intrinsic Debye length, $\lambda=N_a/n_i$, $X=xL_d\sqrt{\ln\lambda/\lambda}$, $Y=yL$ and $(\psi,V,\phi)=(w,v,\varphi)V_{th}\ln\lambda$.

In this paper dimensional voltages and lengths, such as V_{gf} and T_s, are denoted by capital letters. Lower-case letters, v_{gf} and t_s, are used to denote the same quantities non-dimensionalised. Exact analytical solutions to (3) are not available. However, a numerical solution of (3) indicates that a parabolic potential approximation in x is a good approximation for low voltage application. A parabolic potential form in x has been used in [4] to model sub-threshold swing. Here we assume the form

$$w(x,y)=w_0(y)+b(y)x+c(y)x^2 \tag{4}$$

where $w_0(y)$ is the scaled potential along the mid-section, $x=0$.

Using the boundary conditions (2), (3) and (4) gives

$$\begin{cases} b=\dfrac{\varepsilon_{ox}}{2\varepsilon_s}\left(\dfrac{v_{gf}-w_{sf}-\Delta\varphi_f}{t_{oxf}}-\dfrac{v_{gb}-w_{sb}-\Delta\varphi_b}{t_{oxb}}\right)\\ c=\dfrac{\varepsilon_{ox}}{2t_s\varepsilon_s}\left(\dfrac{v_{gf}-w_{sf}-\Delta\varphi_f}{t_{oxf}}+\dfrac{v_{gb}-w_{sb}-\Delta\varphi_b}{t_{oxb}}\right)\end{cases} \tag{5}$$

where the surface potentials are given by,

$$w_{sf}=w_0+b\frac{t_s}{2}+c\frac{t_s^2}{4},\ w_{sb}=w_0-b\frac{t_s}{2}+c\frac{t_s^2}{4} \tag{6}$$

Explicit solutions can be calculated for w_{sf} and w_{sb} from (6):

$$\begin{cases} w_{sf}=\dfrac{\gamma_{s1f}w_0k_{1b}+(V_{gf}-\Delta\varphi_f)k_{2f}+(V_{gb}-\Delta\varphi_b)k_{3b}+\gamma_{s2f}}{k_{4f}}\\ w_{sb}=\dfrac{\gamma_{s1b}w_0k_{1f}+(V_{gb}-\Delta\varphi_b)k_{2b}+(V_{gf}-\Delta\varphi_f)k_{3f}+\gamma_{s2b}}{k_{4b}}\end{cases} \tag{7}$$

where γ_s are the surface potential correction factors and are used as fitting parameters with numerical data, and

$$k_{1i}=1+\frac{t_s\varepsilon_{ox}}{8\varepsilon_s t_{oxi}+3t_s\varepsilon_{ox}} \tag{8}$$

$$k_{2i}=\frac{3t_s\varepsilon_{ox}}{8\varepsilon_s t_{oxi}}-\frac{t_s^2\varepsilon_{ox}^2}{64\varepsilon_s^2 t_{oxf}t_{oxb}+24t_s\varepsilon_s\varepsilon_{ox}t_{oxi}} \tag{9}$$

$$k_{3i}=\frac{3t_s^2\varepsilon_{ox}^2}{64\varepsilon_s^2 t_{oxi}^2+24\varepsilon_s\varepsilon_{ox}t_s t_{oxi}}-\frac{t_s\varepsilon_{ox}}{8\varepsilon_s t_{oxi}} \tag{10}$$

$$k_{4i}=1+\frac{3t_s\varepsilon_{ox}}{8\varepsilon_s t_{oxi}}-\frac{t_s^2\varepsilon_{ox}^2}{64\varepsilon_s^2 t_{oxf}t_{oxb}+24\varepsilon_s\varepsilon_{ox}t_s t_{oxi}} \tag{11}$$

The mid-section electrostatic potential, $w_0(y)$, is determined from the ordinary differential equation:

$$\varepsilon^2\frac{d^2w_0}{dy^2}+Ew_0-\frac{1}{\lambda}e^{(w_0-v)\ln\lambda}+K=0 \tag{12}$$

where

$$E=-\frac{\varepsilon_{ox}}{\varepsilon_s t_s}\left(\frac{k_{1b}}{k_{4f}t_{oxf}}+\frac{k_{1f}}{k_{fb}t_{oxb}}\right) \tag{13}$$

$$\begin{aligned}K=\frac{\varepsilon_{ox}}{\varepsilon_s t_s}\Bigg[&\left(\frac{v_{gf}-\Delta\varphi_f}{t_{oxf}}+\frac{v_{gb}-\Delta\varphi_b}{t_{oxb}}\right)\\&-\frac{(v_{gf}-\Delta\varphi_f)k_{2f}+(v_{gb}-\Delta\varphi_b)k_{3b}}{k_{4f}t_{oxf}}\\&-\frac{(v_{gb}-\Delta\varphi_b)k_{2b}+(v_{gf}-\Delta\varphi_f)k_{3f}}{k_{4b}t_{oxb}}\Bigg]-1\end{aligned} \tag{14}$$

The second derivative terms $b''x$ and $c''x^2$ are neglected in (12); this equation is approximated by its behavior at the mid-section, $x=0$. A typical value of εL is 211.43nm. The long channel approximation of the mid-section potential can be determined from (12) by taking $\varepsilon^2\to 0$, which gives

$$w_0^*=-\frac{lambertW\left(-\theta\dfrac{\ln\lambda}{\lambda E}e^{\left(-\frac{K}{E}-v\right)\ln\lambda}\right)}{\ln\lambda}-\frac{K}{E} \tag{15}$$

where W is the *Lambert function*, see [5]. We adopt $w_0\to w_0^*/\alpha$, where α and θ are the correction factors that we introduced to account for changes in the mid-section potential due to the short channel, parabolic potential approximation and 2-D effects.

$$\alpha = \alpha_0 + \frac{1}{l}(\alpha_1 + \alpha_2 v_{ds}) \text{ and } \gamma_{s2j} = \frac{Kk_{1i}}{\alpha E}(\gamma_{s1j} - 1) \quad (16)$$

where l and v_{ds} are the scaled dimensionless channel length and drain voltage respectively, the fitting parameter α has a very weak dependence on the drain voltage and device channel length (see [2]). The introduction of θ in (15) improves the model accuracy in saturation when different gate voltages applied at the front and back gates.

The total mobile charge per unit gate area for the asymmetric DG MOSFET is given by

$$Q(V) = \varepsilon_{ox}\left(\frac{V_{gf} - \psi_{sf} - \Delta\phi_f}{T_{oxf}} + \frac{V_{gb} - \psi_{sb} - \Delta\phi_b}{T_{oxb}}\right) \quad (17)$$

3 RESULTS AND DISCUSSION

The numerical simulations are obtained for comparison by solving Poisson's equation and the electron continuity equation, as well as the drift–diffusion equation without considering quantum effects using the Sentaurus Device Simulator [3]. The temperature is fixed at 300 K without self-heating. For all simulation results a zero work function difference or flat band voltage is assumed.

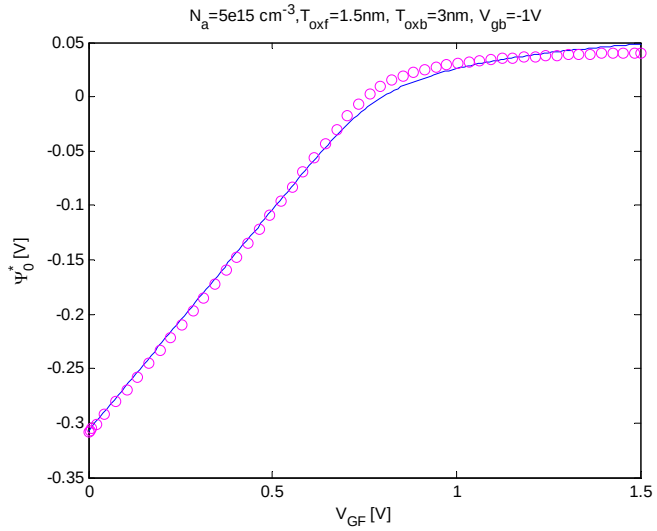

Figure 1: The mid-section potential versus relative front gate voltage for 20nm silicon film, α_0=1.4 and θ=1.5E+7. Circles are numerical and solid line is the compact model.

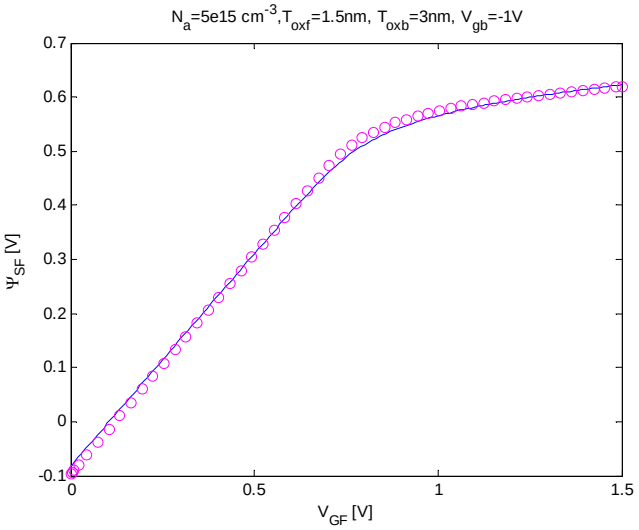

Figure 2: The front gate surface potential versus relative front gate voltage for 20nm silicon film, α_0=1.4 , γ_{s1f}=4 and θ=1.5E+7. Circles are numerical and solid line is the compact model.

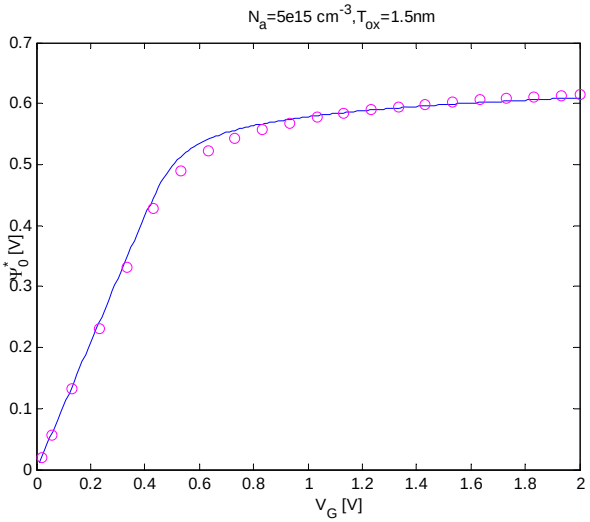

Figure 3: The mid-section potential versus relative gate voltage for 5nm silicon film, α_0=0.96 and θ=1. Circles are numerical and solid line is the compact model.

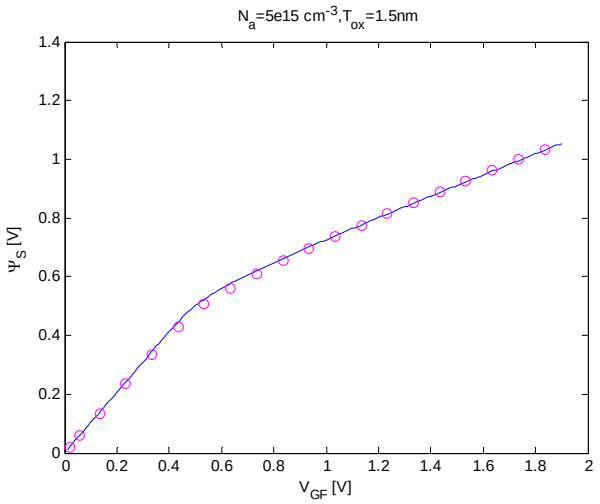

Figure 4: The gate surface potential versus relative gate voltage for 5nm silicon film, α_0=0.96, γ_{s1}=0.83 and θ=1. Circles are numerical and solid line is the compact model.

Figures 1-2 show asymmetric device and Figures 3-4 show the symmetric device simulation results. Our electrostatic potential comparisons in Figures 1-4 indicate that the compact model gives a good approximation. The fact that the fitting parameter θ varies substantially is due to the effect of voltages at the exponent in (15).

REFERENCES

[1] H. Abebe, H. Morris, E. Cumberbatch and V. Tyree, "Compact models for double gate MOSFET with quantum mechanical effects using Lambert function." *Nanotech Proceedings, WCM*, Vol. 3, pp. 849, June 1-5, (2008), Boston, Massachusetts, USA.

[2] H. Abebe, E. Cumberbatch, H. Morris, V. Tyree, T. Numata and S. Uno, "Symmetric and asymmetric double gate MOSFET modeling" *IJSTS*, Institute of Electronics Engineers of Korea, Vol. 9, No. 4, pp. 225-232, Dec. (2009).

[3] *Sentaurus Device User Guide*. Version Z-3.2007, March 2007, Synopsys.

[4] T. K Chiang, "A novel scaling-parameter-dependent subthreshold swing model for double-gate (DG) SOI MOSFETs: including effective conducting path effect (ECPE)" *IOP Semicond. Sci. Technol*. 19, pp. 1386-1390, (2004).

[5] R. Corless, G. Gonnet, D. Hare, D. Jeffrey, and D. Knuth, "On the Lambert W function", Advances in Computational Mathematics 5(4): 329-359 (1996).

[6] H. Lu and Y. Taur, "Physics-Based, Non-Charge-Sheet Compact Modeling of Double Gate MOSFETs," *Nanotech Proceedings, WCM,* pp. 58-62, May 8-12, (2005), Anaheim, CA.

[7] Y. Taur , X. Liang , W. Wang and H. Lu "A continuous, analytical drain-current model for double-gate MOSFETs*," IEEE Electron Device Lett.*, vol. 25, pp. 107, Feb. (2004).

[8] Y. Taur "Analytic solutions of charge and capacitance in symmetric and asymmetric double-gate MOSFET," *IEEE Trans. Electron Devices*, vol. 48, pp. 2861, Dec. (2001).

[9] H. Lu and Y. Taur, "An analytic potential for asymmetric and symmetric Dg MOSFETs," IEEE Trans. Electron Devices, Vol. 53, No. 5, pp. 1161-1168, May (2006).

[10] A.S. Roy, C.C. Enz and J.M. Sallese, "A Charge-Based Compact Model of Double Gate MOSFET," *Nanotech Proceedings, WCM,* Vol. 3, pp. 662, June 1-5, (2006), Boston, Massachusetts, USA.